Desalination and Water Treatment
www.deswater.com
doi:10.5004/dwt.2017.20304

72 (2017) 374–385
April

Novel synthesis of TiO_2 combined spherical carbon for the photocatalytic decolorization of commercial Texbrite dyes under visible light response

Asghar Ali[a], Lei Zhu[a,c], Shu Ye[a], Jin-do Chung[b], Won-Chun Oh[a,*]

[a]*Department of Advanced Materials Science & Engineering, Hanseo University, Seosan 31962, Korea, Tel. +82-41-660-1337, Fax +82-41-688-3352, email: wc_oh@hanseo.ac.kr*
[b]*Department of Environmental Engineering, Hoseo University, Hoseo-ro 79 beon-gil, Baebang-eup, Asan-si, Chungnam, 336-795, Korea*
[c]*Key Laboratory for Advanced Technology in Environmental Protection of Jiangsu Province, Yancheng Institute of Technology, Yancheng 224051, China*

Received 29 February 2016; Accepted 4 November 2016

ABSTRACT

In this work, TiO_2-combined spherical carbon photocatalysts were prepared by using activated carbon and soot as starting material, phenolic resine (PR) as a binder, and TiO_2, TIP as a titanium source. A series of spherical samples (ATP, STP, AOP, SOP) were prepared by controlling the weight percentage of TiO_2 and the binder materials. These spherical samples were characterized via BET, XRD, TEM, AFM, and pressure drop. The photocatalytic activities of the spherical samples (ATP, STP, AOP, SOP) were investigated through the degradation of industrial dyes, including Texbrite BAC-L (TBAC), Reactive black b (RBB), Texbrite MST-L (TMST), and Texbrite BBU- L (TBBU), under irradiation with visible light. Meanwhile, the COD removal effect and the bactericidal effect test were also assessed. The kinetic studies and degradation rate were also conducted in order to determine the order of RBB > TBAC > TMST > TBBU for the industrial dyes.

Keywords: Spherical carbon; TiO_2; Industrial dye; Photocatalytic activities; COD; Bactericidal effect

1. Introduction

The textile, plastics, paper and pulp industries generate streams of waste effluents containing a substantial amount of organic dye pollutants, and these are usually not biodegradable and are very difficult to remove. Furthermore, discharging them into water bodies without prior treatment can cause havoc on the environment. The molecules in these effluents usually possess carcinogenic and mutagenic properties that not only harm aquatic or marine ecosystems, but also actively or passively become a major threat to human life [1,2].

Various physical, chemical, and biological methods [3] have been employed to treat such dyes, including coagulation, flocculation, precipitation, ozonation, oxidation [4] and radiation [5]. However, the high operating cost, sludge production, and complexity of the treatment processes limit their applicability. The purification of waste water through the photocatalytic degradation of dyes using semiconductor particles has been proven to be a very effective method that leads to the complete mineralization of the pollutants [6–8]. The excitation of direct band-gap semiconductors under light irradiation leads to the generation of electron-hole pairs, some of which eventually diffuse out to the surface of the crystals and react with donors or acceptors from their surroundings, resulting in photocatalysis [9].

Titanium dioxide (TiO_2) has been extensively used as a photocatalyst for solar energy conversion and environmental applications (water and air purification) because of its good photoactivity, high chemical stability, low cost, and nontoxicity, and several attempts have been adopted to improve the photocatalytic performance of TiO_2, such as immobilization of the TiO_2 powder onto supports,

*Corresponding author.

such as activated carbon fiber (ACF) [10] and activated carbon (AC) [11–14]. AC is highly adsorptive due to the pore structure that it develops, resulting in a high specific area. Moreover, the particle size of commercial AC is usually in the micro-scale range [15]. AC must have medium surface area and porosity to facilitate the diffusion of pollutants and to release the products from the surface; so many researchers have reported a synergistic effect for AC-supported TiO_2 systems, such as a high photocatalytic activity, photosensitivity and high adsorptive ability. Activated carbon increases the photodegradation rate by progressively allowing an increased quantity of substrates to come into contact with titania through means of adsorption. This is important because the oxidizing species (·OH) generated by the photocatalyst does not migrate very far from the active centers of the titania, and therefore degradation only takes place on the surface of the catalyst. Oh et al. first pointed that the adsorption of the pollutant was transfered by a common interface from AC to TiO_2 [16].

Activated carbon fibers (ACFs) and granular activated carbons (GACs) are the most widely used activated carbon materials. However, spherical activated carbons (SACs) have recently received a considerable amount of attention for their various advantages over ACFs and GACs [16,17]. Spherical activated carbons (SACs), in comparison to commonly-used cylindrical activated carbon granules, ensure better column packing, which implies higher efficiency in removing impurities from water. Moreover, an adsorbent with a spherical shape is more resistant to abrasion, reduces the resistance to the flow of liquids, and endows the activated carbon with better mechanical properties [17].

Chemical oxygen demand (COD) widely used to characterize polluting aqueous effluents. It indicates the amount of oxygen required for complete oxidation of a wastewater sample, and it is widely used to control the degree of pollution in water and to manage effluent quality [18] COD, which represents the total pollution load for most wastewater discharge [19], is a main index that assesses organic pollution in aqueous systems [20]. Typically, COD is determined by organic compounds present in the water sample that are completely oxidized by adding a strong oxidant, usually $K_2Cr_2O_7$ or $KMnO_4$ [21], and then calculating the result according to the quantity of oxidant consumed, expressed in terms of its oxygen equivalence.

In this paper, TiO_2-combined spherical carbon photocatalysts (T-SCPs) are prepared starting from spherical carbon from powdered coal, a binder additive, and titanium oxide or Titanium isopropoxide (TIP). We used different raw carbon materials and TiO_2 precursor materials to produce four kinds of T-SCPs (ATP, STP, AOP, SOP) and compared their photocatalytic activity under irradiation with visible light through the degradation of industrial dyes, including Texbrite BAC-L(TBAC), REACTIVE BALCK B (RBB), Texbrite MST-L (TMST), and Texbrite BBU-L (TBBU).

2. Experiment procedure

2.1. Materials

The main materials were coal-based activated carbon with size of 100–400 mesh and charcoal, provided by Hanil Green Tech (Korea). Phenolic rosin (PR) was used as a bonding agent and was purchased from Kangnam Chemical Co., Ltd (Korea). Alcohol (95%) was used as a dispersing agent, and was purchased from Samchun Pure Chemical Co., Ltd (Korea). Titanium oxide (TiO_2) and Titanium isopropoxide (TIP) were purchased from Duksan Pure Chemical Co., Ltd (Korea). Four types of dyes Texbrite BAC-L (TBAC), Reactive Black B (RBB), Texbrite MST-L (TMST), and Texbrite BBU-L (TBBU) were used as model pollutant and were purchased from Samchun Pure Chemical Co., Ltd, (Korea) and Texchaem Co. Ltd (Korea), and their chemical structure shown in Fig. 1. We designed a shaped mould, shaker sieve and shaker to prepare and form the spherical carbons, and these machines as well as the prepared samples are shown in Fig. 2a and 2b.

2.2. Preparation of TiO_2 combined spherical carbon (T-SCPs)

The T-SCPs production consists of three stages: formation, carbonization and activation.

2.2.1. Formation of T-SCPs

First, activated carbon/soot, PR and TiO_2 or TIP were mixed with 20–30% alcohol. The mixture was then placed into the shaped mould to form agglomerates. To produce spheres of these agglomerates, a shaker and a sieve with size of 30–50 mesh were used with a shaking rate of 50 round/min at 80–90°C. After shaking for 10–15 min, the agglomerates formed spheres and dried in the activated carbon powder at 100–200°C.

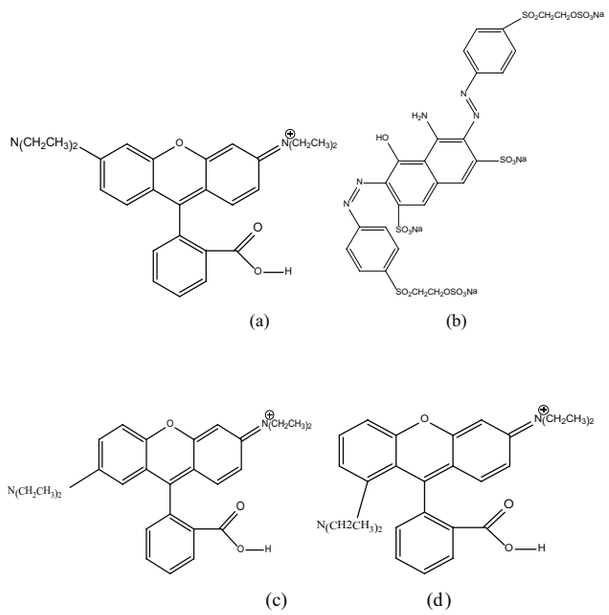

Fig. 1. Chemical structure of four types of dyes (a) Texbrite BAC-L(TBAC), (b) Reactive Black B (RBB), (c) Texbrite MST-L (TMST) and (d) Texbrite BBU-L (TBBU).

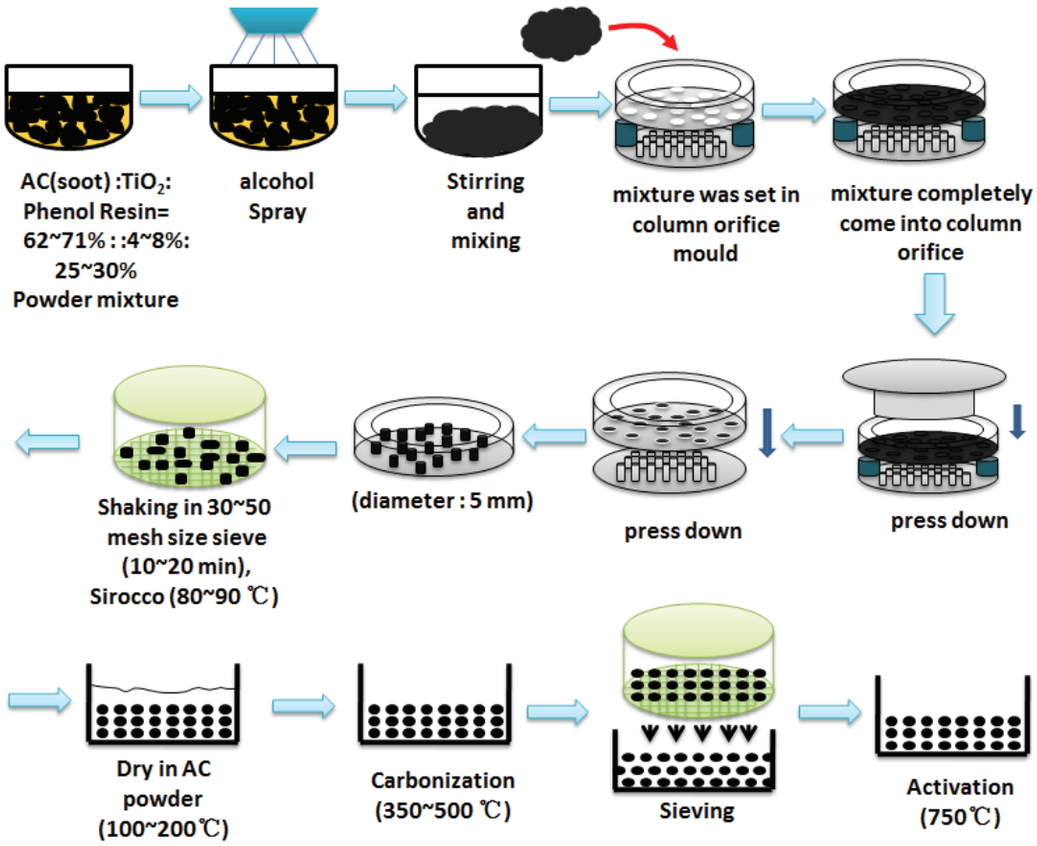

(a)

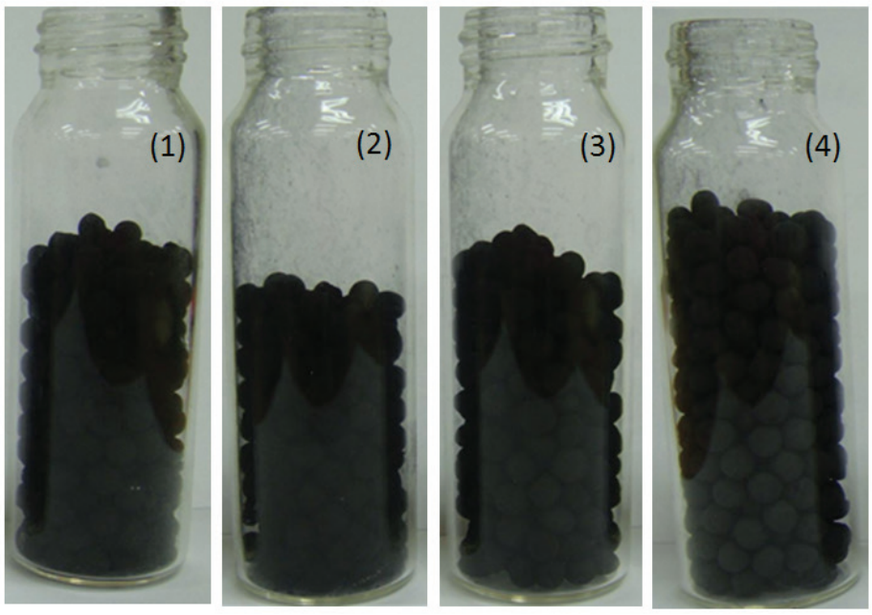

(b)

Fig. 2. (a) The manufacture procedure of TiO_2 combined spherical carbon; (b) Appearance images of TiO_2 combined spherical carbon photocatalysts: (1) ATP, (2) STP, (3) AOP and (4) SOP.

2.2.2. Carbonization and activation

In the first part of this experiment, the agglomerates were formed into spherical shapes. These spherical agglomerates were heat-treated in activated carbon powder at 350–500°C for 1 h with a heating rate of 6°C/min to form SACs. Then, the sample of heat-treated SACs was heated in an inert atmosphere with N_2 at a flow rate of 150 mL/min at 700°C for 2 h. Then, the carbonized agglomerate was heated with CO_2 at a flow rate of 150 mL/min at about 950°C for 2 h with a heating rate of 10°C/min. We conducted a comparison by preparing four kinds of samples with different amounts of activated carbons and PR. The manufacturing procedure for the T-SCPs and the preparation conditions with the sample codes are shown in Fig. 2a and listed in Table 1, respectively.

2.3. Characterization

The surface morphology and structure of the T-SCPs was examined in TEM (JSM-5200, JEOL, Japan). XRD was used to identify the crystal phase of the SACs, and the XRD patterns were obtained at room temperature with a Shimata XD-D1 (Japan) using CuKα radiation. The BET surface area of the SCPs was measured using a Quantachrome surface area analyzer (Monosorb, USA).

2.4. Strength measurement

Strength measurement was determined based on JIS R 721227 by using one-point bending (Instron 4201) with a support distance of 30 mm/min and cross head speed of 0.5 mm/min. The diameter size of the sample was of about 5 mm, and the strength density was calculated using the following equation:

$$\sigma F = 3PL/2BD^2$$

where σF is the strength density (kg/m^2), P is the breaking load (kg), L is the support distance (cm), B is the width of sample (cm) and D is the thickness of the sample (cm).

2.5. Visible light photodegradation of commercial Texbrite dyes

Photochemical data are obtained to describe the behavior of commercial Texbrite dyes (TBAC, RBB, TMST, and TBBU) degraded by the SCPs samples in a 100 mL glass container with visible light irradiation (Fawoo, Lumidas-H, 8W, Korea). The differences in the photocatalytic activity are investigated by selecting a different sample amount and dye concentration. The reactor was placed for 2 h in a dark box for the T-SCPs composite particles to adsorb the TBAC, RBB, TMST, and TBBU molecule maximum, which was hereafter considered as the initial concentration (c_0) after dark adsorption. After adsorption, visible light irradiation was restarted to proceed with the degradation reaction. The degradation of commercial Texbrite dyes (TBAC, RBB, TMST, and TBBU) was carried out in a glass reactor (bottom area = 20 cm^2), and samples were regularly withdrawn from the reactor, and the dispersed powders were removed through a centrifuge. The concentration of dye in the solution was determined as a function of the irradiation time, and the solution was then withdrawn regularly from the reactor at 30 min, 60 min, 90 min, and 120 min. The photocatalytic behavior of the samples was analyzed via absorbance spectrometry with a UV/Vis spectrophotometer (Optizen POP, Mecasys, Korea).

Table 1
The preparation methods and nomenclature

Preparation method	Nomenclature
AC : TiO_2 : PR = 65 : 5 : 30	ATP
Soot : TiO_2 : PR = 70 : 5 : 25	STP
AC : TIP : PR = 65 : 5 : 30	AOP
Soot : TIP : PR = 70 : 5 : 25	SOP

*AC : Activated carbon, PR : Phenol resine, TOS : Titanium isopropoxide.

2.6. COD test

The photocatalytic activity was also tested by measuring the degradation of piggery waste in aqueous media in a 100 mL glass container with an irradiation system with 20W UV light at 365 nm in a dark box. The suspended sample (0.5 g) was kept at 0.01 g/ml, and then the suspended solution was placed in the dark for at least 2 h to establish an adsorption-desorption equilibrium, which was hereafter considered as the initial concentration (c_0) after dark adsorption. The experiments were then carried out under irradiation with visible light, the reactor was placed on a magnetic churn dasher, and the measurements were taken at 300 min. The samples were withdrawn regularly from the reaction, and dispersed powders were removed using a centrifuge. Clean transparent solutions were then tested with a COD cell test photometer.

2.7. Antibacterial effects

To detect the antibacterial effects, the T-SCPs series spherical samples were treated with different weight amounts of Ag^+ (6, 8, 10%) and a fixed spherical sample of AOP. The treated samples were then used as bactericide and were denoted as Ag6, Ag8, and Ag10. The halo test was employed using the Berman method [22], and the bactericidal activities against *E. Coli* and *S. Aureus* were examined in a cultivated culture medium. The quantitative analysis of the bactericidal effects was conducted using the flask shaking method [23]. In our previous studies [24,25], the bactericidal activity levels of Ag6, Ag8, and Ag10 materials against *E. Coli* and *S. Aureus* were investigated in detail using the flask shaking method. The bactericidal activity against the strain used herein was examined in a cultivated culture medium. For the test, 300 mL of prepared trypticase soy broth (TSB badge, ca. 120°C, 15 min) were first sterilized. Then, each badge strain was cultivated for 24 h under conditions with constant humidity at a temperature of 37°C. After culturing, a phosphate buffer solution was added to the cultured solution, and the strain in the solution was then counted again. The Ag6, Ag8, and Ag10 samples were

then dispersed into the counted strain solution both with and without sunlight. After dispersion and irradiation, the number of bacteria was counted as a function of time, and the process was carried out again after 120 min under constant humidity and temperature.

3. Results and discussion

3.1. Textural characterization of T-SCPs

Fig. 3 shows the XRD pattern of the T-SCPs, and the results indicate that the mixed phase transition of the four kinds of T-SCPs (ATP, STP, AOP and SOP) have rutile and anatase phase. According to previous studies, both anatase and rutile phase can improve the photocatalytic activity [10]. The peaks corresponding to the anatase TiO_2 phase appeared at 25.3, 37.5, 48.0, 54.9, and 62.5, which match the diffractions of the (101), (004), (200), (211), and (204) planes of anatase, thus indicating that the prepared TiO_2 existed in the anatase phase. The 2θ values of 27.52°, 36.20°, 41.44° and 54.48° correspond to the (110), (101), (111) and (211) crystal planes of rutile TiO_2 [26] due to the anatase and rutile phase that can be easily generated after carbonization and activation at a high temperature above 600°C [27,28].

Fig. 4 shows a TEM image of the TiO_2 combined spherical carbon (T-SCPs) samples. The TEM analysis was carried out to further study the microscopic structural information between AC and TiO_2, as shown in Fig. 4a–d. Fig. 4a and 4c were taken with small magnification so that the large surface structure and the overall history of the nanoparticles were exposed. These images indicate that the TiO_2 nanoparticles are well-distributed, mixed with AC and binder materials. The overall picture indicates much less agglomeration of the nanoparticles. However, Fig. 4b and 4d exhibit a different morphology from that in 4a and 4c, with more agglomeration observed after using soot as the carbon material, which further confirms using AC as the carbon material could lead to a better morphology and relatively good particles dispersion [27]. The HRTEM image (Fig. 4e) indicates the

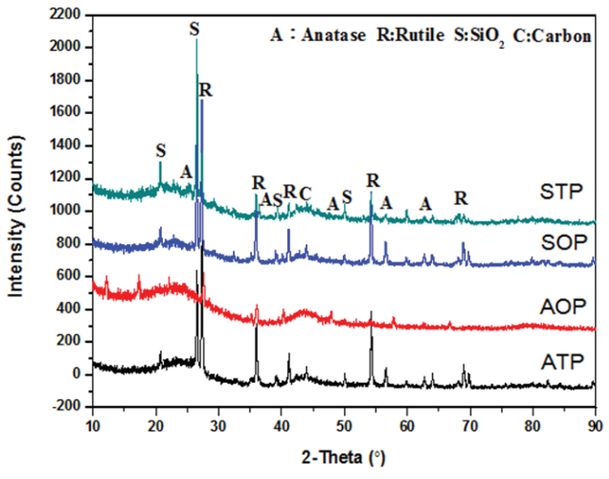

Fig. 3. XRD patterns of TiO_2 combined spherical carbon photocatalysts.

lattice spacing of TiO_2 and AC bending materials, which are of approximately 0.357, 0.176 and 0.134 nm respectively. Fig. 4f shows the AFM results for the ATP sample with a similar morphology as that seen in Fig. 4a. Oh [28] provided a report indicating that the good dispersion of small particles could provide more reactive sites for reactants than aggregated particles.

Fig. 5a shows the changes in the BET surface area of the SCPs before and after activation. Compared to ATP, the surface area of the AOP is clearly seen to increase before activation, while it is different after activation. The TiO_2 introduced into the pores of the active carbon can be considered to have decreased the BET surface area. However, the surface area of the STP and SOP decreased little, which may be the result of the presence of TiO_2 having an effect on the pore type and pore volume of the composites. Moreover, a comparison with the surface area before activation shows that the BET surface area of the SCPs improved much more after activation, by about 2–3 times. The TiO_2 and PR can be considered to have clogged little by little in the pores of the activated carbon or soot. Comparing the ATP or AOP samples with the STP or AOP samples shows that the BET surface of the AC based samples is much larger than that of the soot based samples before and after activation due to activated carbon having a larger surface area and pore volume than soot. Activated carbon is actually oxidized charcoal, and the pores give activated carbon a massive surface area that allows it to absorb organic chemicals and some other stuff.Furthermore Fig. 5b and 5c exhibit the N_2 adsorption/desorption mode, and corresponding pore size distribution curves of TiO_2 combined spherical carbon sample, N_2 adsorption/desorption isotherm of AOP and SOP composite shows a typical IV curve with a hysteresis loop, and the isotherm of STP is of the type II (BDDT), evident that the presence of large mesopores and macropores [29]. However ATP shows typical type IV behavior with H_3 hysteresis-loop [30] and the pore size distribution of the AOP and SOP (Fig. 5c) is extend from 1 nm to 12 nm and has different distinct positions, while STP and ATP are broad from 1 nm to 11 nm and 5 nm to 100 respectively. This illustrates Table 2.

Fig. 6 shows the strength intensity values of the T-SCPs samples after activation. The results clearly show that the strength values of the T-SCPs increase with an increasing amount of PR. This indicates that the bonding agent has a significant influence on the strength of the T-SCPs, and that if the spherical shapes formed well, the strength value is also high. Fig. 6 shows that the strength after activation for ATP and AOP is greater than that of STP and SOP due to the content of PR decreasing from 30% to 25%.

3.2. Visible light photocatalytic decomposition of commercial Texbrite dyes

To study the photocatalytic effect of the prepared AOP sample, we investigated the decomposition reaction of TBAC, RBB, TMST, and TBBU in water under irradiation with visible light. The experiments were performed to study the variations in the rate of photodegradation with different catalyst amounts of 0.02, 0.03 and 0.05 g for four kinds of commercial Texbrite dye (TBAC, RBB, TMST, and TBBU) solutions with concentration of 2×10^{-5} mol/L, which obey

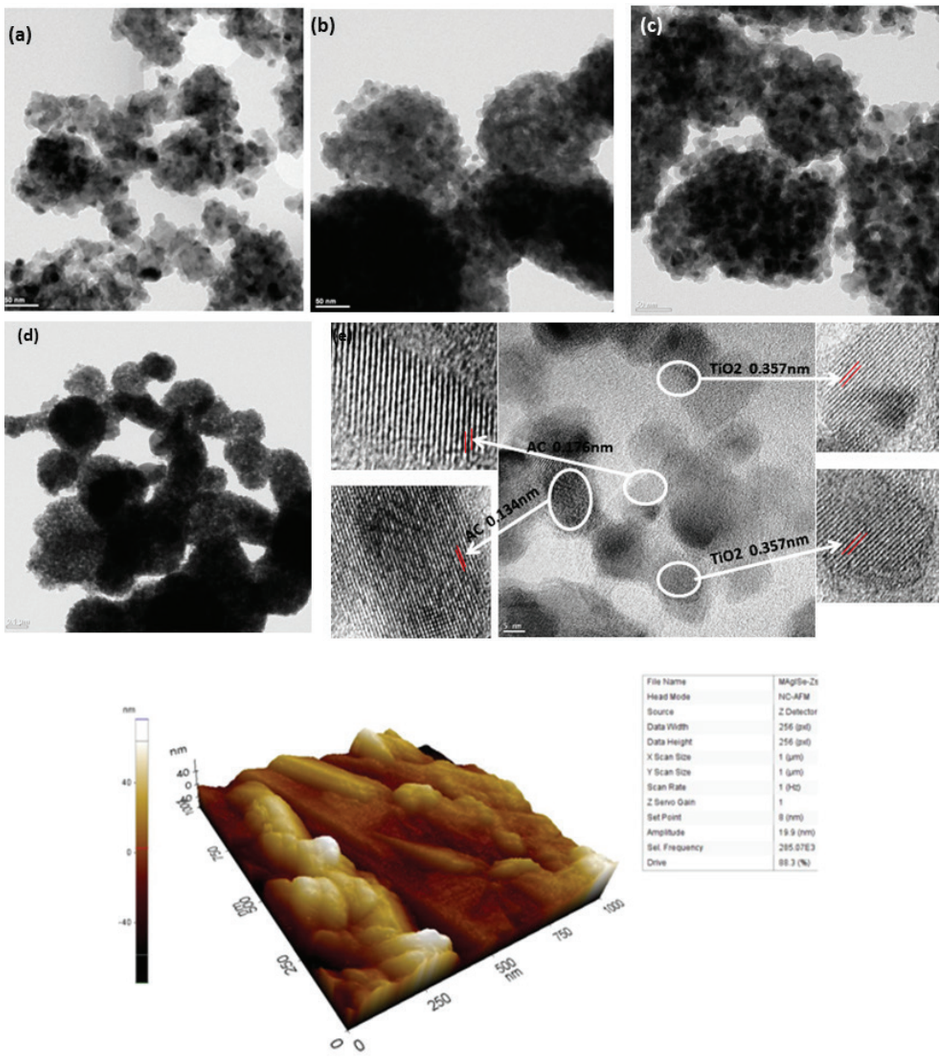

Fig. 4. TEM images of TiO_2 combined spherical carbon photocatalysts; (a) ATP, (b) STP, (c) AOP and (d) SOP; (e) HRTEM image (5 nm) of TiO_2 and AC binding materials and, (f) AFM images of TiO_2 combined spherical carbon photocatalyst (ATP).

the pseudo-first-order kinetics with respect to the concentration of commercial Texbrite dyes:

$$-d_c/d_t = k_{app}c$$

The integration of the equation (with the restriction of $c = c_{ads}$ at $t = 0$, with cads being the initial concentration in the bulk solution after dark adsorption and t reaction time) will lead to the following expected relation:

$$-\ln(c/c_{ads}) = k_{app}t$$

where c and c_{ads} are the reactant concentrations at time t = t and t = 0, respectively, k_{app} and t are the apparent reaction rate constant and time, respectively. According to the equation, a plot of $-\ln(c/c_{ads})$ versus t will yield a slope of k_{app}. The results are displayed in Fig. 7, from which the degradation efficiency of commercial Texbrite dye solution can be observed to increase sharply with the catalyst amount. This is due the increase in number of available adsorption and catalytic sites on the surface of the AOP sample [25]. The degradation rate constant for RBB reaches 7.94×10^{-3} min^{-1} under irradiation with visible light, and it was much higher than the corresponding values for TBAC (6.13×10^{-3}), TMST (5.08×10^{-3}), and TBBU (4.21×10^{-3}). The result indicates that the optimum catalyst amount is 0.05 g.

The effect of the commercial Texbrite dye concentration on the degradation efficiency was investigated by varying the concentration from 1 to 3×10^{-5} mol/L under irradiation with visible light for 120 min with a catalyst amount of 0.05 g. The degradation rate constant

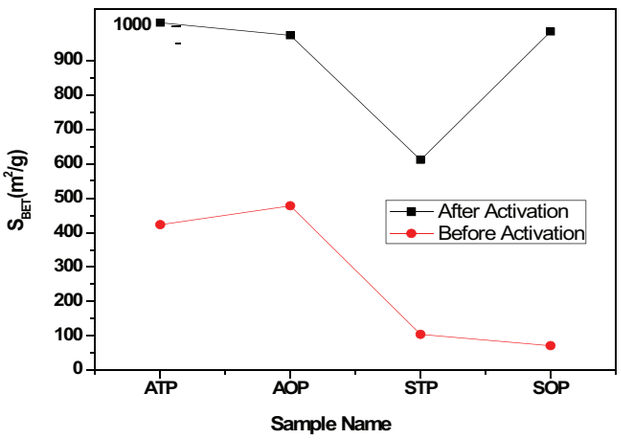

(a)

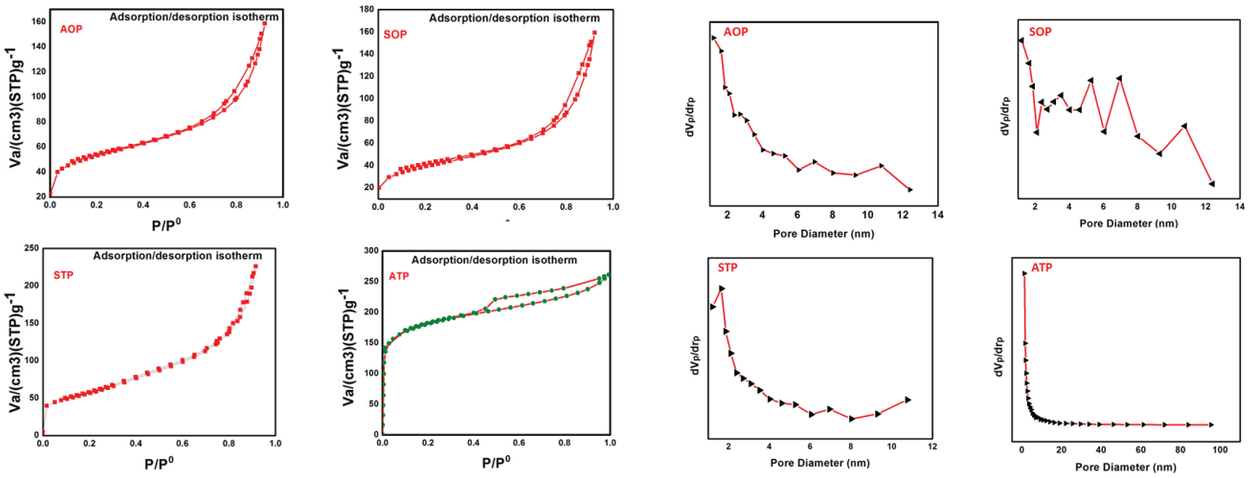

(b) (c)

Fig. 5. (a) BET surface area, (b) N_2 adsorption and desorption isotherm of ATP, STP, AOP, SOP and (c) pore size distribution for spherical carbon containing of Titania.

Table 2
Some surface area parameters for spherical activated carbon

Sample	SBET ($m^2 g^{-1}$)	Pore volume (p/p_0 = 0.921) ($cm^3 g^{-1}$)	Average pore diameter (nm)
ATP	1010	0.3548	7.2145
STP	611.0	0.3496	7.1114
AOP	972.0	0.2454	5.2973
SOP	984.0	0.2462	7.1596

for RBB reaches 9.93 × 10^{-3} min^{-1} under irradiation with visible light, when the concentration is 1 × 10^{-5} mol/L, and the other results are depicted in Fig. 8. It is clear that the degradation efficiency decreases as the concentration increases. The presumed reason is that a mass of visible light may be absorbed by the dye molecules in aqueous solution rather than the catalyst particles for a high concentration, which can reduce the efficiency

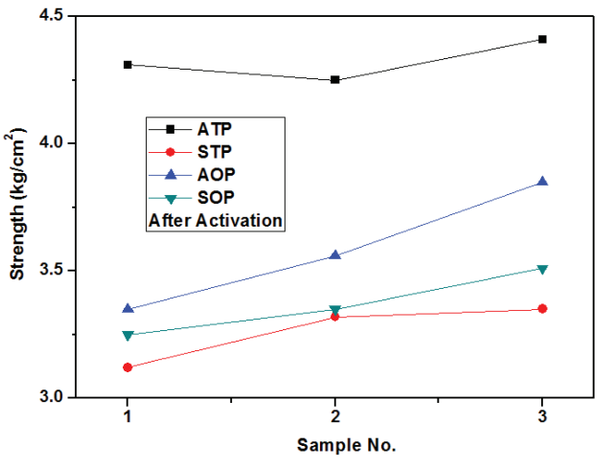

Fig. 6. The strength intensity of TiO_2 combined spherical carbon photocatalysts.

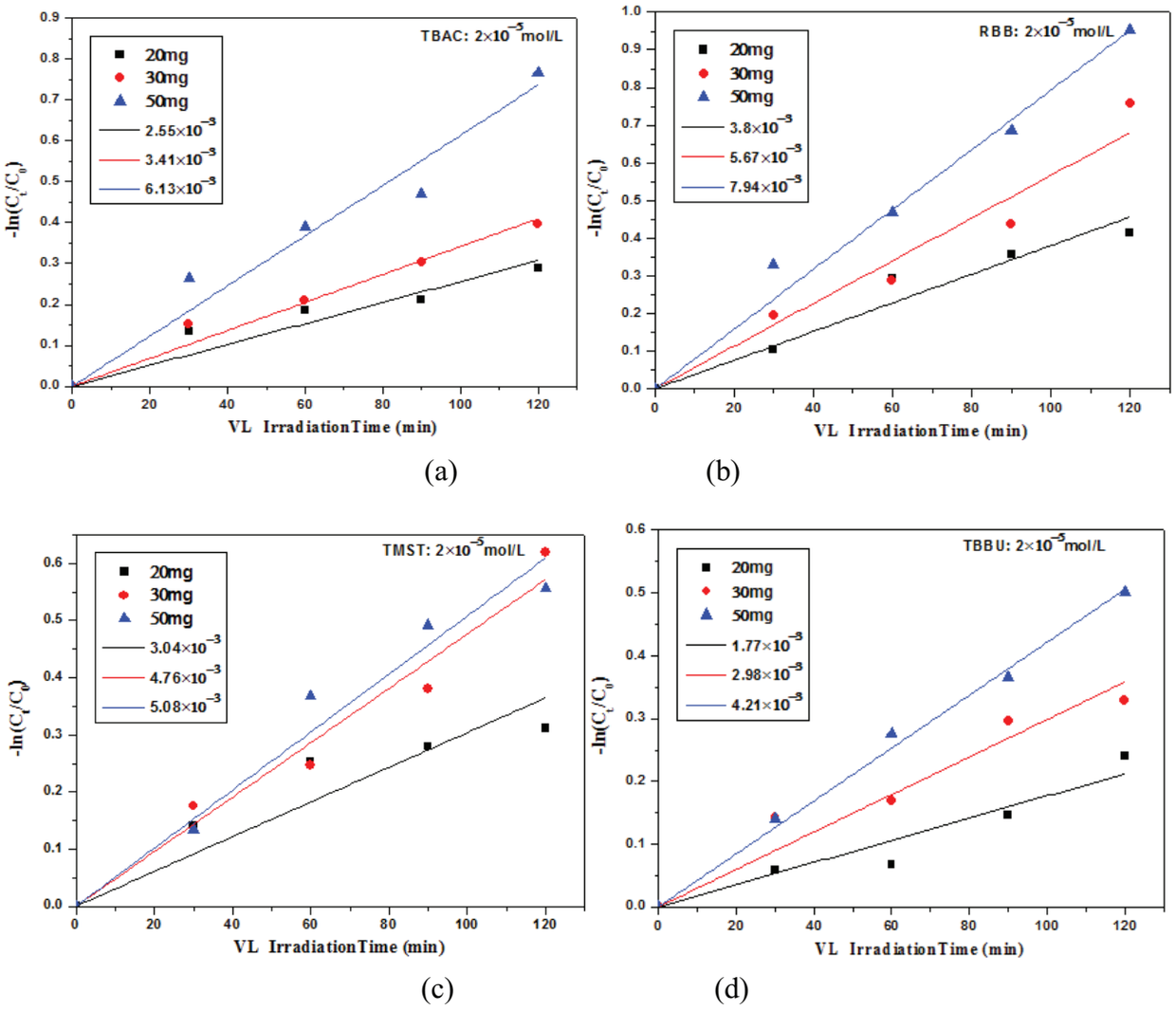

Fig. 7. Sample amount effect for (a) TBAC, (b) RBB, (c) TMST, and (d) TBBU degradation under visible light irradiation (20, 30, 50 mg, 2×10^{-5} mol/L).

of the catalytic reaction. Another possible reason is the intermediate products that formed upon the photocatalytic degradation of the dye might compete with the dye molecules for the limited adsorption and catalytic sites on the surface of the catalyst particles, thus inhibiting the degradation of the dye to a certain extent.

The photocatalytic activity stability and cycle performance are further demonstrated with circulating runs in the photocatalytic degradation of commercial Texbrite dyes (TBAC, RBB, TMST, and TBBU) in the presence of the AOP sample. As shown in Fig. 9, the photocatalyst does not exhibit any significant loss of photocatalytic activity after four runs under irradiation with visible light, which indicates that the as-prepared AOP sample has high stability and cannot be photocorroded during the photocatalytic oxidation of the dye molecules. This result is significant for practical applications since the improvement in catalytic activity with visible light and the prevention of catalyst deactivation will lead to more cost-effective operation.

3.3. COD effect of T-SCPs

The chemical oxygen demand (COD) refers to the oxygen required for complete oxidation of a wastewater sample. Note that the direct photolysis of infect ants accompanies the reduction of COD, implying oxidation ability. Evidently, the COD reduction can only be preceded via photocatalytic oxidation, so more active sites of the T-SCPs are advantageous to the oxidation reaction [31]. As is shown for different T-SCPs Fig. 9, the removal percentage of the COD for the ATP and AOP samples is relatively high at about 70 to 80% due to greater competition of the intermediates for oxi-

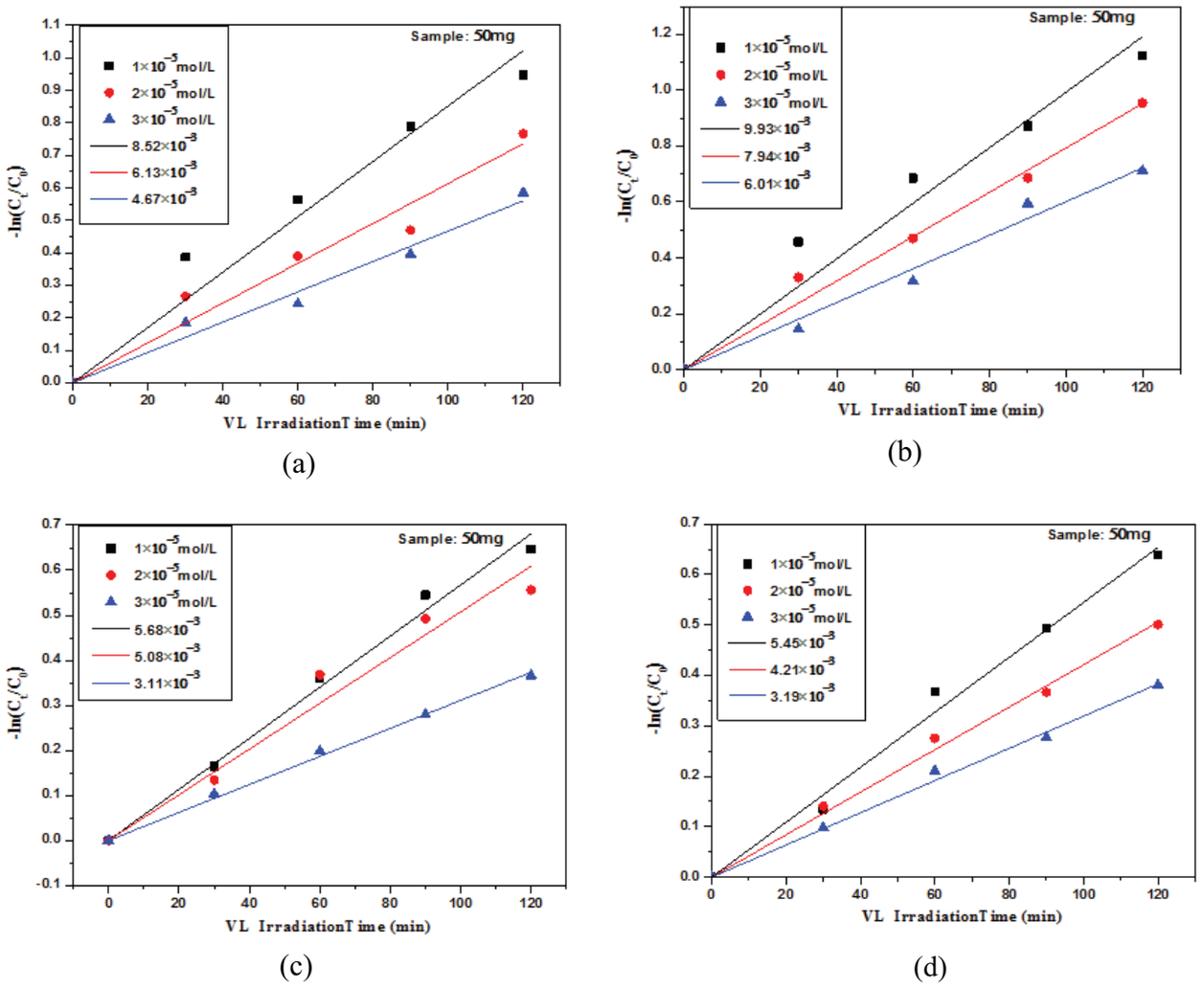

Fig. 8. Industrial dye concentration effect for (a) TBAC, (b) RBB, (c) TMST, and (d) TBBU degradation under visible light irradiation (50 mg, 1, 2 and 3 × 10^{-5} mol/L).

dative species. Fig. 9 shows that the removal percentage of COD increased with an increase in the amount of soot compared to active carbon, and the total removal percentage of STP is bigger than that of the ATPs. This means that the reactor that contains the STP samples has relatively strong oxidation ability.

3.4. Antibacterial activity

The antibacterial activity of the spherical T-SCPs series samples against *E. Coli* was investigated due to its ample availability and ubiquitous presence, as shown in Fig. 11a. For comparison, we used the Kanamycin antibiotic given in the culture media of the bacteria as standard. In Fig. 11a, the AOP sample can be seen to efficiently restrict the growth of the bacterial colonies, with antibacterial activity that reaches 90%. The detailed antibacterial activity is investigated by treating the as-prepared spherical AOP samples with different amounts of Ag^+, from 6% to 10%, and the results are shown in Fig. 11b. The results indicate that the use of a proper amount of Ag^+ in the composites can promote a better bactericidal effect [32]. According to the results shown in Fig. 11b, a clear but smaller inhibition zone around 0.9 cm of *E. Coli* and 0.55 cm of *S. Aureus* for Ag10 was observed, indicating the existence of a slight antibacterial effect against *E. Coli* and *S. Aureus* for the Ag series spherical samples.

4. Conclusions

In this study, TiO_2-combined spherical shaped carbon photocatalysts (T-SCPs) were successfully prepared, and among these the AOP sample exhibits the best spherical shapes and visible light photocatalytic activity. The TEM measurements

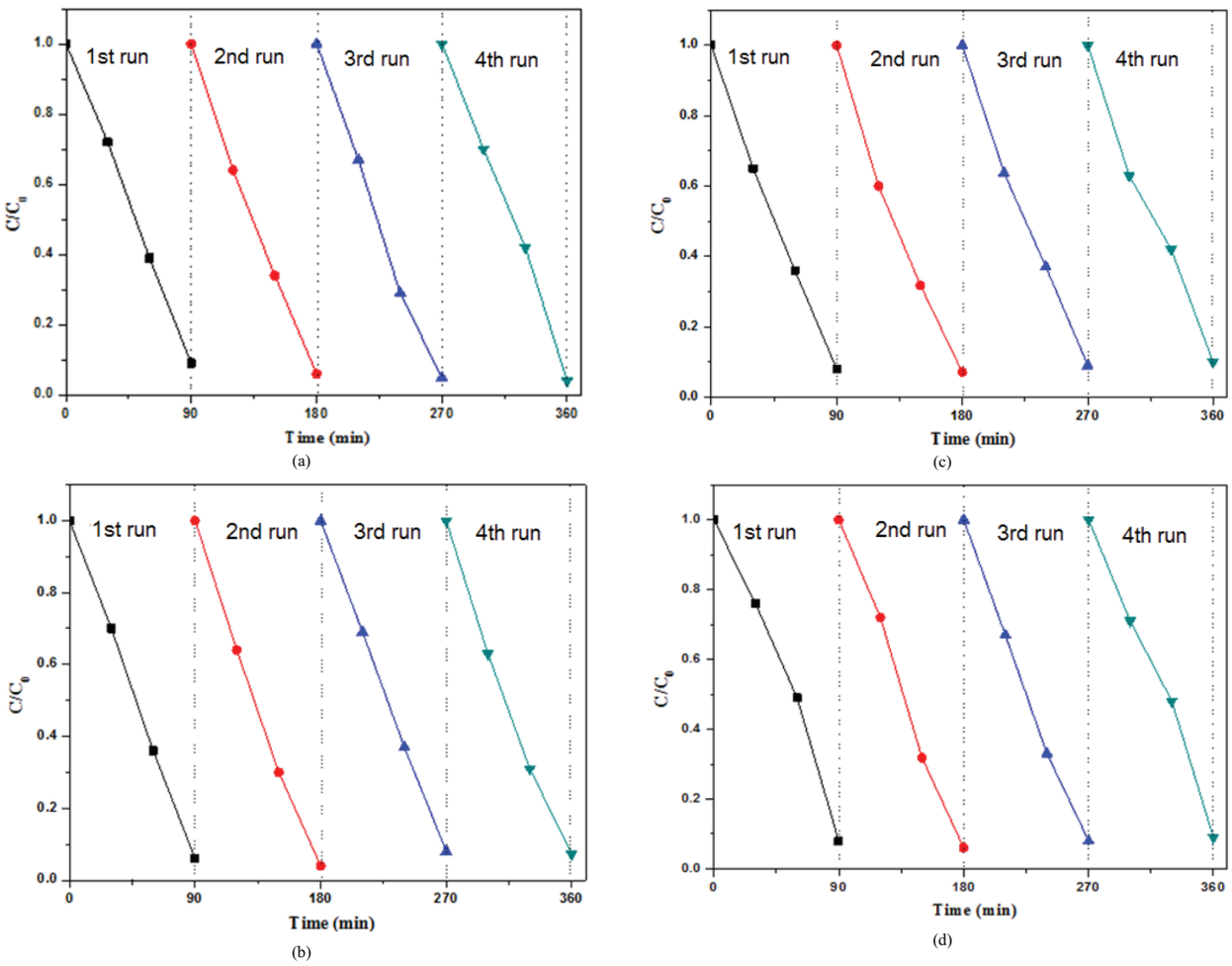

Fig. 9. Cycling runs about the photocatalytic activity under visible light irradiation for (a) TBAC, (b) RBB, (c) TMST, and (d) TBBU (50 mg, 2×10^{-5} mol/L).

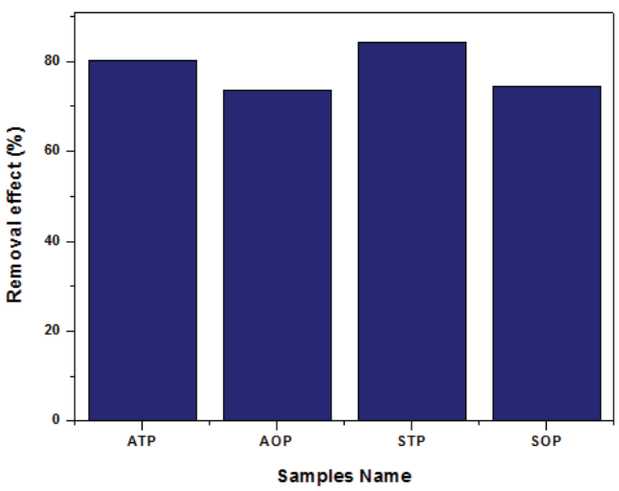

Fig. 10. COD removal effect (%) of TiO_2 combined spherical carbon photocatalysts.

show that the SCP composites were synthesized by immobilizing the TiO_2 particles on the surface of coal based materials. The XRD result shows that the prepared T-SCPs samples consisted of a pure anatase phase. After the activation of the T-SCPs composites, the BET surface area increased, and the strength intensity of the AC based SCPs was higher than that of soot based SCPs. The degradation rate constant for RBB reaches 7.94×10^{-3} min^{-1} under irradiation with visible light, which was much higher than the corresponding values for TBAC (6.13×10^{-3}), TMST (5.08×10^{-3}), and TBBU (4.21×10^{-3}). The removal percentage of COD increased with an increase in the amount of soot compared with active carbon, and the total removal percentage of STP is bigger than that of ATPs. Finally, the use of a proper amount of Ag^+ in the spherical carbon can be seen to promote a better bactericidal effect.

Acknowledgments

This work was supported by the Human Resources Development program of the Korea Institute of Energy

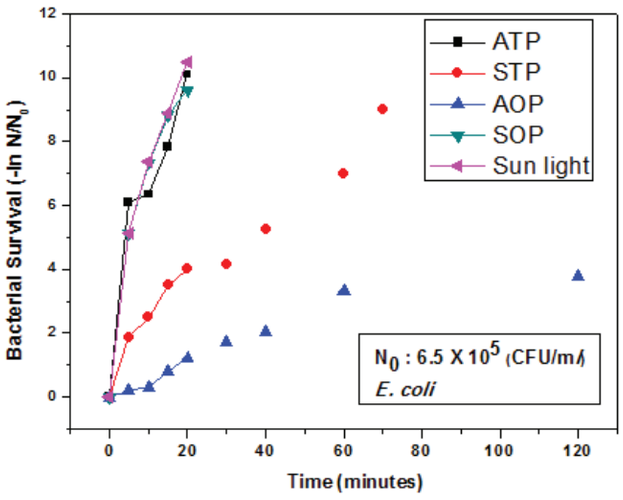

(a)

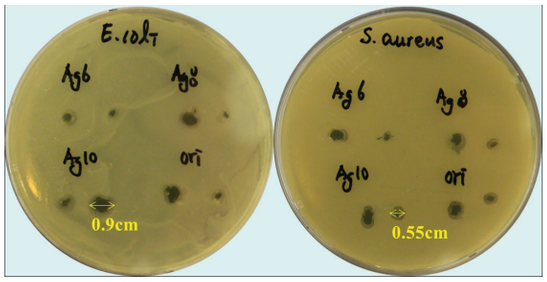

(b)

Fig. 11. Bactericidal effects of (a) TiO_2 combined spherical carbon photocatalysts; (b) Ag-TiO_2 combined spherical carbon photocatalysts (*E. coli*, *S. Aureus*).

Technology Evaluation and Planning (KETEP) grant, funded by the Korea Government Ministry of Trade, Industry, and Energy and a Chung Nam Green Environment Center grant research fund in 2015.

References

[1] A. Cesaro, V. Naddeo, V. Belgiorno, Wastewater treatment by combination of advanced oxidation processes and conventional biological systems, J. Bioremed. Biodeg., 4 (2013) 208–215.
[2] C.T. Helmes, C.C. Sigman, V.A. Fung, K. Thompson, M.K. Doeltz, M. Mackie, T.E. Klein, D. Lent, A study of azo and nitro dyes for the selection of candidates for carcinogenic bioassay, J. Environ. Sci. Health., A19 (1984) 97–231.
[3] M.B. Pazarbasi, A. Kocyigit, G. Ozdemir, I. Yasa, I. Karaboz, Decolorization of various leather dyes and leather industry effluent by Trametestrogii TEM H2, Fresen. Environ. Bull., 21 (2012) 1410–1416.
[4] M.A. Rauf, M.A. Meetani, A. Khaleel, A. Ahmed, Photocatalytic degradation of Methylene Blue using a mixed catalyst and product analysis by LC/MS, Chem. Eng. J., 157 (2010) 373–378.
[5] M. Aliabadi, H. Ghahremani, F. Izadkhah, T. Sagharigar, Photocatalytic degradation of N-methyl-2-pyrrolidone in aqueous solutions using light sources of UVA, UVC and UVLED, Fresen. Environ. Bull., 21 (2012) 2120–2125.
[6] E. Hu, X. Wu, S. Shang, X.M. Tao, S.X. Jiang, L. Gan, Catalytic ozonation of simulated testile dyeing wastewater using mesoporous carbon aerogel supported copper coxide catalyst, J. Cleaner Prod., 112 (2016) 4710–4718.
[7] A. Khataee, R.D.C Soltani, A. Karimi, S.W. Joo, Sonocatalytic degradation of a textile dye over Gd-doped ZnO nanoparticles synthesized through sonochemical process, Ultrason. Sonochem., 23 (2015) 219–230.
[8] A. Fujishima, T.M. Rao, D.A. Tryk, Titanium dioxide photocatalysis, J. Photochem. Photobio., C1 (2000) 1–21.
[9] H. Zhang, C. Hu, Effective solar absorption and radial micro channels of SnO_2 hierarchical structure for high photocatalytic activity, Catalysis Comm., 14 (2011) 32–36.
[10] W.C. Oh, J.S. Bae, M.L. Chen, Characterization of AC/TiO_2 composite prepared with pitch binder and their photocatalytic activity, Bull. Kor. Chem. Soc., 27 (2006) 1423–1428.
[11] R. Leary, A. Westwood, Carbonaceous nanomaterials for the enhancement of TiO_2 photocatalysis. Carbon, 49 (2011) 741–772.
[12] S.X. Liu, X.Y. Chen, X. Chen, A TiO_2/AC composite photocatalyst with high activity and easy separation prepared by a hydrothermal method, J. Hazard. Mater., 143 (2007) 257–263.
[13] M.L. Chen, J.S. Bae, W.C. Oh, Characterization of AC/TiO_2 composite prepared with pitch binder and their photocatalytic activity, B. Kor. Chem. Soc., 27 (2006) 1423–1428.
[14] M. Ouzzine, A.J. Romero-Anaya, M.A. Lillo-Rodenas , A. Linares-Solano, Spherical activated carbon as an enhanced support for TiO_2/AC photocatalysts, Carbon, 67 (2014) 104–118.
[15] C. Djilani, R. Zaghdoudi, F. Djazi, B. Bouchekima, A. Lallam, A. Modarressi, M. Rogalski, Adsorption of dyes on activated carbon prepared from apricot stones and commercial activated carbon, J. Taiwan Inst. Chem. Eng., 53 (2015) 112–121.
[16] W.C. Oh, J.G. Kim, H. Kim, M.L. Chen, F.J. Zhang, K. Zhang, J.G. Choi, Ze-Da Meng, TiO_2 combining spherical activated carbon photocatalysts and their physicochemical and photocatalytic activity, Kor. J. Mater. Res., 20 (2010) 535–542.
[17] J.B. Yang, L.C. Ling, L. Liu, F.Y. Kang, Z.H. Huang, H. Wu, Preparation and properties of phenolic resin based activated carbon spheres with controlled pore size distribution, Carbon, 40 (2002) 911–916.
[18] W.C. Oh, W.B. Ko, Physical properties of K-activated carbon and its removal efficiencies for chemical factors, J. Ind. Eng. Chem., 12 (2006) 373–379.
[19] Q. Yang, Z. Liu, J. Yang, Simultaneous determination of chemical oxygen demand (COD) and biological oxygen demand (BOD5) in wastewater by near-infrared spectrometry, J. Water. Res. Prot., 1 (2009) 286–289.
[20] K.Q. Bao, J.Q. Gao, Z.B. Wang, R.Q. Zhang, Z.Y. Zhang, N. Sugiura, Enhanced removal of chemical oxygen demand, nitrogen and phosphorus using the ameliorative anoxic/anaerobic/oxic process and micro-electrolysis, Water. Sci. Technol., 66 (2012) 850–857.
[21] L. Wang, Y.Z. Peng, J. Ma, Y. Liu, N.P. Ma, Effects of COD/TN and HRT(s) on nutrients removal by an alternating anoxic/oxic CAST, Huan. Jing. Ke. Xue., 31 (2010) 2370–2375.
[22] E. Berman, Toxic metals and their analysis, chapter 4, Heydenand Son, London, UK. 1980.
[23] W.C. Oh, W.C. Jang, Physical properties and biological effects of activated carbon fibers treated with the herbs, Carbon, 41 (2003) 1737–1742.
[24] W.C. Oh, Surface transition by solvent washing effects and biological properties of metal treated activated carbons, Bull. Korean Chem. Soc., 25 (2004) 639–646.
[25] W.C. Oh, A.R. Jung, W.B. Ko, Characterization and relative photonic efficiencies of a new nanocarbon/TiO_2 composite photocatalyst designed for organic dye decomposition and bactericidal activity, Mater. Sci. Eng., C4 (2009) 1338–1347.
[26] S.H. Joo, S.J. Choi, I. Oh, J. Wak, Z. Liu, O. Terasaki, R. Ryoo, Ordered nanoporous arrays of carbon supporting high dispersions of platinum nanoparticles, Nature, 412 (2001) 169–172.

[27] L. Zhu, Z.D. Meng, M.L. Chen, F.J. Zhang, J.G. Choi, J.Y. Park, W.C. Oh, Photodegradation of MB solution by the metal (Fe, Ni and Co) containing AC/TiO_2 photocatalyst under the UV irradiation, J. Multifunct. Mater. Photosci., 1 (2010) 69–76.
[28] W.C. Oh, J.S. Bae, M.L. Chen, Preparation of carbon-coated TiO_2 at different heat treatment temperatures and their photoactivity, Carbon Sci., 7 (2006) 259–265.
[29] W. Tu, Y. Zhou, Q. Liu, S, yan, S. Bao, Xia. wang, M. Xiao, Z. Zou, In situ simultaneous reduction-hydrolysis technique for fabrication of TiO_2-graphene 2D sandwich-like hybrid nanosheets: graphene-promoted selectivity of photocatalytic-driven hydrogenation and coupling of CO_2 into methane and ethane. Adv. Funct. Mater., 23 (2013) 1743–1749.
[30] B. Li, T. Liu, Y. Wang, Z. Wang, ZnO/graphene-oxide nanocomposite with remarkably enhanced visible-light-driven photocatalytic performance, J. Colloid Interface. Sci. 377 (2012) 114–121.
[31] R. Devi, R.P. Dahiya, Chemical oxygen demand (COD) reduction in domestic wastewater by fly ash and brick kiln ash, Water. Air. Soil. Pollut., 174 (2006) 33–46.
[32] Q.L. Feng, J. Wu, G.Q. Chen, F.Z. Cui, T.N. Kim, J.O. Kim, A mechanistic study of the antibacterial effect of silver ions on escherichia coli and staphylococcus aureus, J. Biomed. Mater. Res., 52 (2000) 662–668.